Supporting Information

Unraveling Confined Dynamics of Guests Trapped in Self-Assembled Pd_6L_4 Nanocages by Ultrafast mid-IR Polarization Dependent Spectroscopy

*Rahul Gera, Stephen L. Meloni, Jessica M. Anna**

University of Pennsylvania, 231 South 34 Street, Philadelphia, Pennsylvania 19104, United States.

Contents:

1. Details of Steady State and Time-Resolved Spectroscopic Measurements:

NMR Measurements:

^{1}H NMR spectra were recorded on a Bruker DMX360 at 360 MHz at 298 K in $CDCl_3$ for **1** and **2** and D_2O for **1** $\subset$ **A**, **1** $\subset$ **B**, **2** $\subset$ **A**, and **2** $\subset$ **B**.

Steady State UV/VIS Absorption Measurements:

Absorption measurements were carried out with a JASCO V-750 spectrophotometer. Absorption spectra were obtained in a quartz sample cell with a 1 mm pathlength. UV/VIS spectra were recorded with 2 nm resolution with one scan cycle.

Steady State Infrared Absorption Measurements:

FTIR spectra were carried out with a JASCO FT/IR-4600 spectrometer. FTIR spectra were collected with a sample cell consisting of two 1 mm thick calcium fluoride windows separated by a ~150-micron Teflon spacer. This sample cell was also used for the ultrafast measurements. The FTIR spectra reported were obtained with 2 cm^{-1} resolution and averaging a total of 40 scans. FTIR measurements were performed before and after the ultrafast measurements to confirm the integrity of the host-guest complex.

Mid-IR Polarization Dependent Pump-Probe Measurements:

To perform the ultrafast mid-IR polarization dependent pump-probe measurements 60% of the output of a 800 nm 100 fs 1 kHz 4W Ti:Sapphire regenerative amplifier (Coherent Libra) was used to pump a commercial two stage optical parametric amplifier (Coherent TOPAS C). The resulting signal and idler were difference frequency mixed in a commercial DFG resulting in a tunable mid-IR output. To probe the carbonyl stretching modes of the metal carbonyl complexes mid-IR pulses centered at 2000 cm^{-1} with a bandwidth of ~80 cm^{-1} were generated. Given the bandwidth of the pulses generated with the commercial DFG, only the terminal carbonyl stretching modes were probed for the ultrafast measurements. Following the DFG, a calcium fluoride wedge splits the mid-IR output into two paths with 96% of the transmitted beam acting as the pump and the 4% reflection acting as the probe. A mechanical chopper operating at 500 Hz was placed into the pump arm to chop every other laser pulse. A $\lambda/2$ waveplate was placed in the path of the pump beam to adjust the polarization. Holographic wire grid polarizers (Thorlabs WP25H-C) were placed in the pump and probe arms to ensure the purity of the polarizations for all experiments. Pump and probe beams were focused by an off-axis parabolic mirror and overlapped temporally and spatially at the sample position using a 50 μm pinhole. After passing through the sample, the probe beam was collimated with an off-axis parabolic mirror and transmitted through a wire grid polarizer acting as an analyzer. The probe beam was directed into a Horiba iHR320 spectrometer. The signal was dispersed with a 50 g/mm grating blazed for 6 μm and imaged onto a single row of a commercial 2 X 64 element Mercury Cadmium Telluride (MCT) detector interfaced with a FPAS spectrograph (Infrared Systems Development). The time delay between the pump and the probe pulses was controlled by varying the pump pathlength using a motorized translation stage (Newport ILS250CCL). FTIR measurements were performed before and after the ultrafast measurements to confirm the integrity of the host-guest complex.

The temporal width of the mid-IR pulses was measured by performing PG-FROG using a 2 mm thick germanium window. The temporal width of the mid-IR pulses was found to be ~120 fs (FWHM).

2. Synthesis Protocol for the Pd_6L_4 Nanocages:

Nanocages **A** and **B** were prepared according to Fujita *et al. Nature* **1995**, *378*, 469; Kusukawa *et al. J. Am. Chem. Soc.*, **2002**, 124, 13576; and Gera *et al. J. Am. Chem. Soc.*, **2014**, 136, 15909.[1-3] The starting materials (ethylene diamine, palladium chloride, 2,4,6-tri-4-pyridyl-1,3,5-triazine, deuterium oxide (D_2O)) and all solvents and reagents were purchased from Sigma-Aldrich Co., Tokyo Chemical Industry Co. Ltd., and Fisher Scientific.

Fig. S1 displays the ^{1}H NMR of nanocage **A** along with a schematic representation of the cage. The ^{1}H NMR (360 MHz, D_2O, 298 K) of cage **A** has signals at the following: δ 9.09 (d, 24H, pyridine-α, cage A), 8.59 (d, 24H, pyridine-β, cage A), 2.93 (s, 24H, -CH_2-, cage A). The ^{1}H NMR matches that of the reported nanocage **A** in Fujita *et al. Nature* **1995**, *378*, 469, confirming the synthesis of the nanocage.[1] Fig. S2 displays the ^{1}H NMR of the nanocage **B** along with a schematic representation. The ^{1}H NMR (360 MHz, D_2O, 298 K) of cage **B** has signals at the following: δ 9.44 (d, 24H, pyridine-α, cage B), 8.89 (d, 24H, pyridine-β, cage B), 8.47 (d, 12H, Ha, cage B), 8.37 (t, 12H, Hb, cage B), 7.68 (d, 12H, Hd, cage B), 7.58 (t, 12H, Hc, cage B). The ^{1}H NMR matches that of the reported nanocage **B** in Kusukawa *et al. J. Am. Chem. Soc.*, **2002**, 124, 13576, confirming the synthesis of the nanocage.[2]

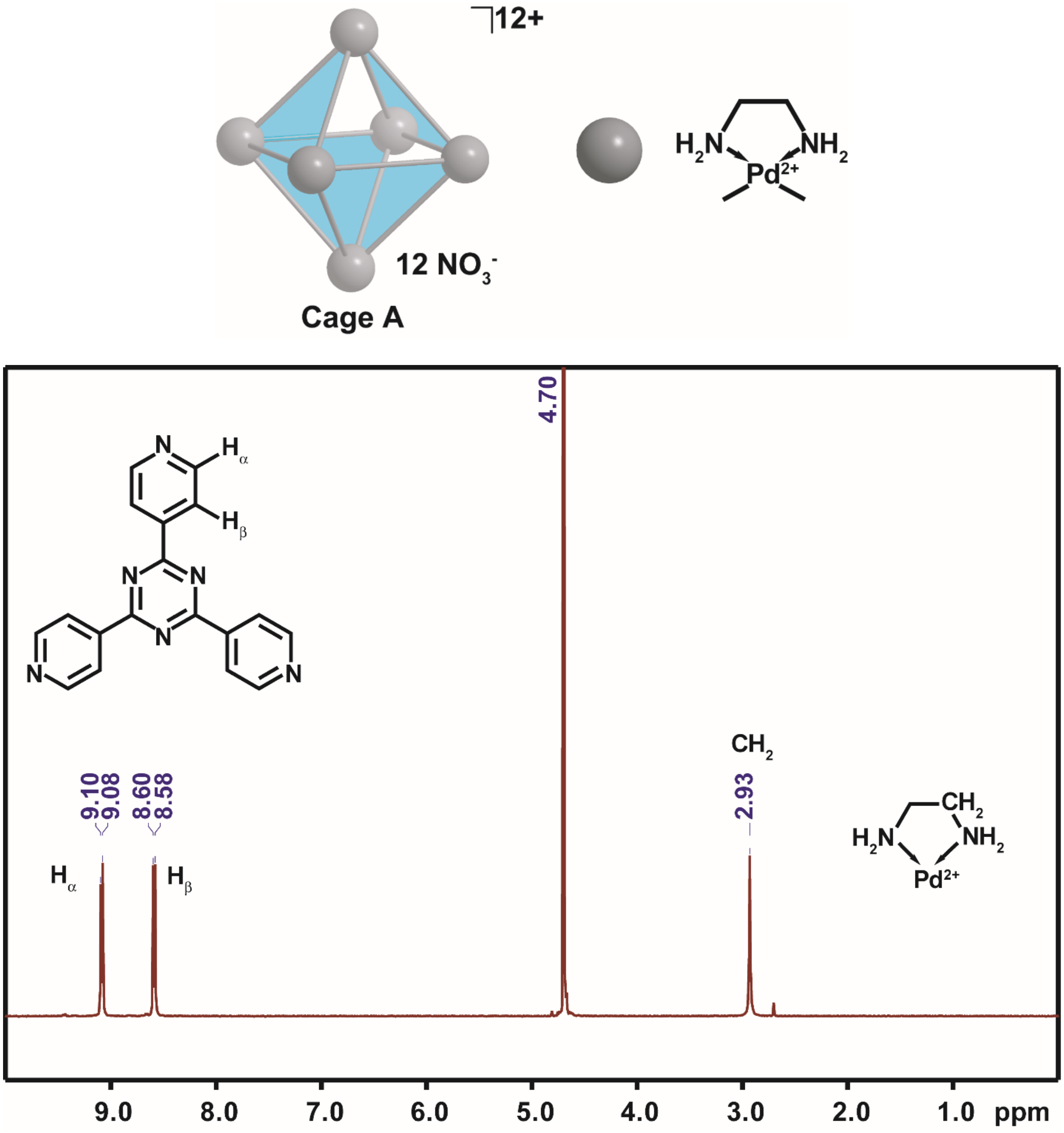

Figure S1. The ^{1}H NMR spectrum (360 MHz, D$_2$O, 298 K) of cage **A**. The ^{1}H NMR spectrum is consistent with the previously reported ^{1}H NMR spectrum of nanocage **A** (Fujita *et al*. *Nature* **1995**, *378*, 469).

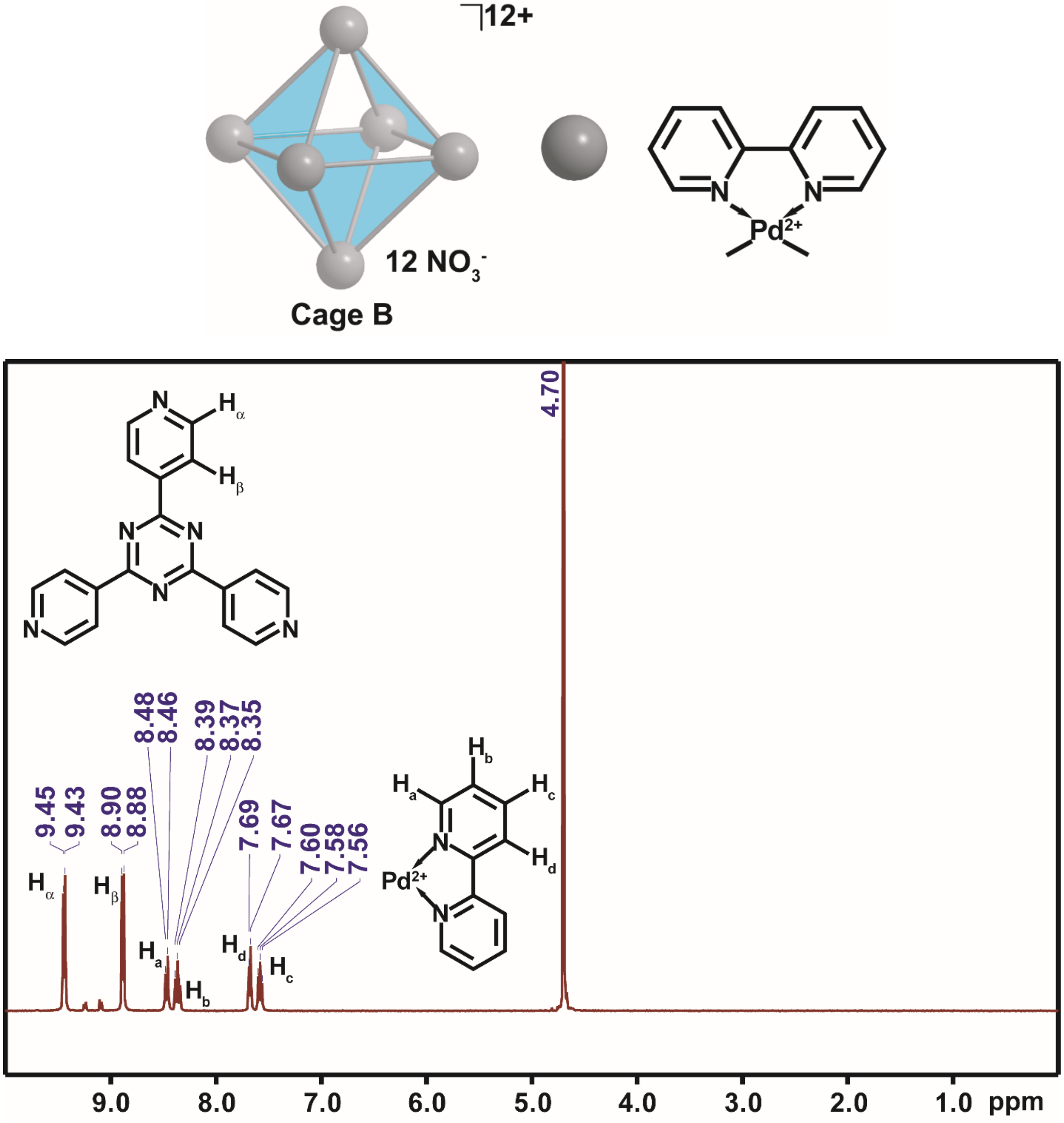

Figure S2. The ^{1}H NMR spectrum (360 MHz, D_2O, 298 K) of cage **B**. The ^{1}H NMR spectrum is consistent with the previously reported ^{1}H NMR spectrum of nanocage **B** in Kusukawa *et al*. *J*. *Am*. *Chem*. *Soc*., **2002**, 124, 13576.

3. Synthesis Protocol for the Host-Guest Complexes:

The metal carbonyl guests, (Bis(cyclopentadienyl ruthenium dicarbonyl) dimer), **1**, and (Cyclopentadienyl iron (II) dicarbonyl dimer), **2**, were purchased from Sigma-Aldrich and used as obtained. The host-guest complexes were prepared by slightly modifiying the protocol for insertion of guest **1** in Pd_6L_4 based nanocages reported in Horiuchi *et al. J. Am. Chem. Soc.*, **2011**, 133, 12445. For all host guest complexes syntheiszed, the integrity and purity of the samples in D_2O were confirmed through ^1H NMR. Encapsulation of the metal carbonyl complexes by the cage is confirmed by an observation of upfield shifts of the metal-carbonyl signals in the ^1H NMR spectrum.[4] Details for synthesis of each host-guest complex follow.

Synthesis of 1 ⊂ A

22.2 mg of **1** was suspended in a 1 ml D_2O solution of cage **A** (5 mM). The resulting solution was stirred at room temperature for 1 h, and the the transparent cage **A** solution turned reddish. Residual ruthenium complex was removed with a 0.45 μm filter. The resulting solution was characterized through ^1H NMR and FTIR spectroscopy. The ^1H NMR spectrum is consisiteint with the the previously reported host-guest complex (Horiuchi *et al., J. Am. Chem. Soc.*, 2011, 133, 19691) with the exception of the extra methyl groups on the amine skeleton which are absent in our ethylenediamine complex.[4] Fig. S3 displays a shematic strucutre of **1** ⊂ **A** along with the ^1H NMR of **1** ⊂ **A** (360 MHz, D_2O, 298 K): δ 9.11 (d, pyridine-Hα, cage A), 8.59 (d, pyridine-Hβ, cage A), 3.38 (s, Cp, guest 1), 2.92 (s, $-CH_2-$, cage A).

Synthesis of 2 ⊂ A

17.7 mg of **2** was suspended in a 1 ml D_2O solution of cage **A** (5 mM) and the resulting solution was stirred at room temperature for 1 h, the transparent cage **A** solution turned reddish. Residual iron complex was removed with a 0.45 μm filter. The resulting solution is carried forward for further characterization through ^1H NMR and FTIR spectroscopy. Fig. S4 displays a schematic respresentation of **2** ⊂ A along with the ^1H NMR of **2** ⊂ A (360 MHz, D_2O, 298 K): δ 9.10 (broad d, pyridine-Hα, cage A), 8.59 (broad d, pyridine-Hβ, cage A), 2.92 (s, $-CH_2-$, cage A).

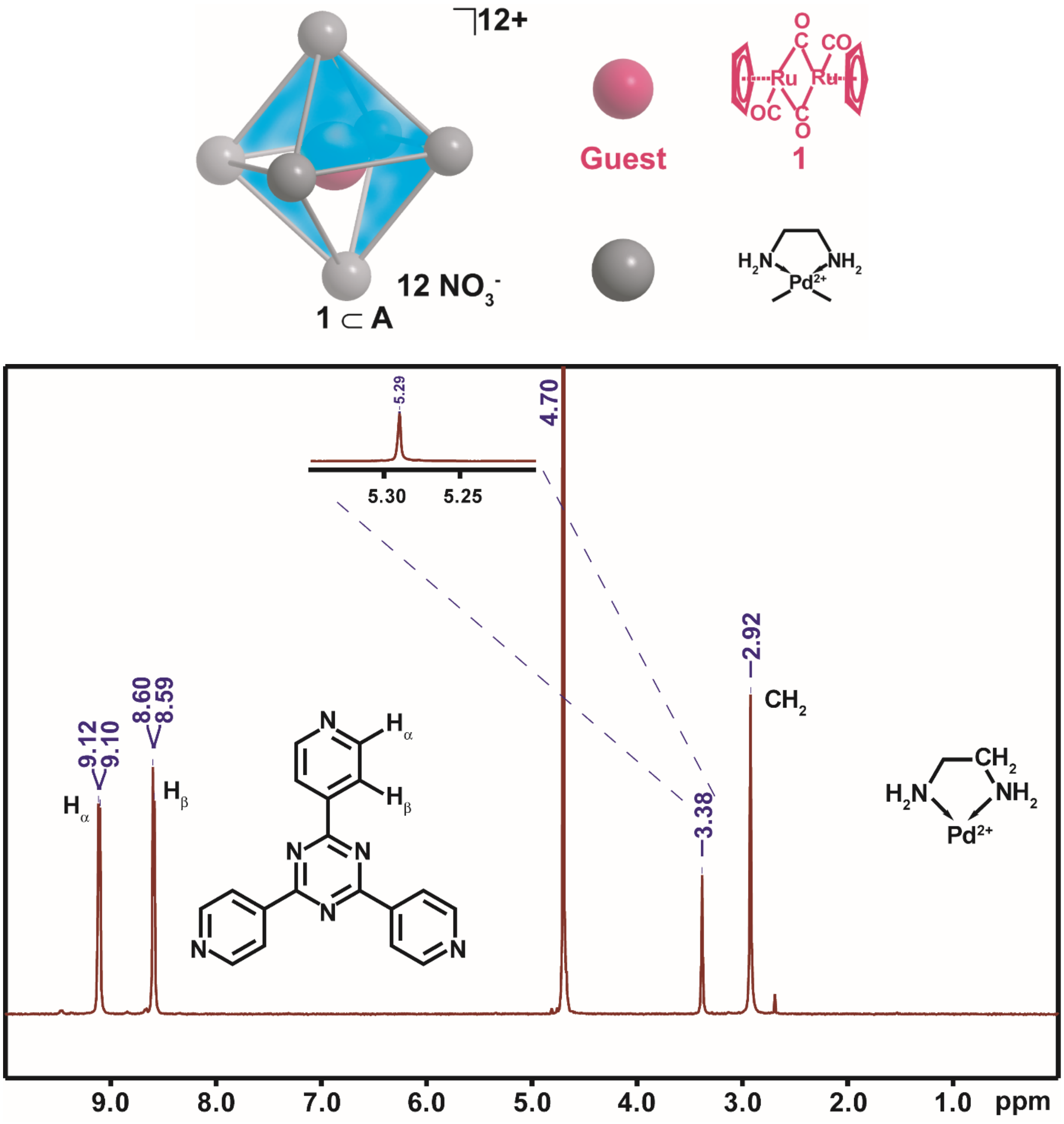

Figure S3. ^{1}H NMR spectrum of **1** ⊂ **A** (360 MHz, D$_2$O, 298 K). Proton signals of **1** free in CDCl$_3$ (δ = 5.29 ppm, shown in inset) shift upfield, δ = 3.38 ppm (Δδ = 1.91 ppm) when **1** is encapsulated by cage **A** The ^{1}H NMR spectrum is consistent with previously reported ^{1}H NMR spectra of similar host-guest complexes[4] with a difference lying in the extra methyl groups on the amine skeleton which are absent in our ethylenediamine cage complex.

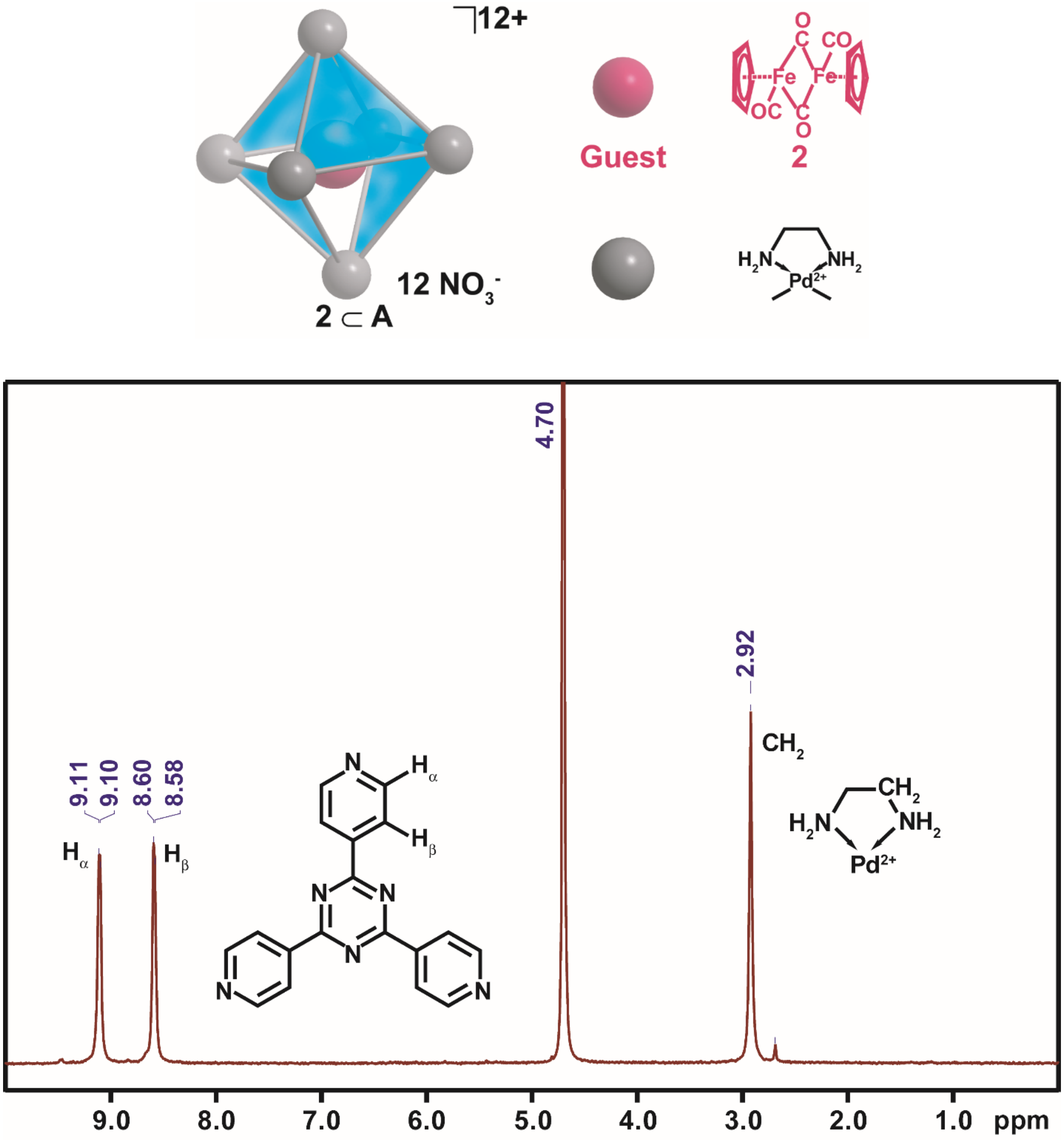

Figure S4. ^{1}H NMR spectra of **2** ⊂ **A** (360 MHz, D_2O, 298 K). The proton signal from **2** disappears when it forms a complex with cage **A**. The ^{1}H NMR signals of the cage broaden, possibly due to a spin change of the guest. This would be expected when a paramagnetic species is trapped inside the cage.

Synthesis of $\mathbf{1} \subset \mathbf{B}$

22.2 mg of **1** was suspended in a 1 ml D_2O solution of cage **B** (5 mM) and the resulting solution was stirred at room temperature for 1 h, the pale yellow cage **B** solution turned reddish. Residual ruthenium complex was removed with a 0.45 μm filter. This solution is carried forward for further characterization through ^1H NMR and FTIR spectroscopy. The ^1H NMR is consisteint with the reported NMR spectrum of the complex (Horiuchi *et al., J. Am. Chem. Soc.*, 2011, 133, 19691) with the only exception of the extra methyl groups on the amine skeleton which are absent in our bipyridine complex.[4] Fig. S5 displays a schematic representation of $\mathbf{1} \subset \mathbf{B}$ along with the ^1H NMR of $\mathbf{1} \subset \mathbf{B}$ (360 MHz, D_2O, 298 K): δ 9.46 (d, pyridine-Hα, cage B), 8.89 (d, pyridine-Hβ, cage B), 8.46 (d, Ha bipyridyl, cage B), 8.36 (t, Hb bipyridyl, cage B), 7.69 (d, Hd bipyridyl, cage B), 7.57 (t, Hc bipyridyl, cage B), 3.54 (s, Cp, guest **1**).

Synthesis of $\mathbf{2} \subset \mathbf{B}$

17.7 mg of **2** was suspended in a 1 ml D_2O solution of cage **B** (5 mM) and the resulting solution was stirred at room temperature for 1 h, the pale yellow cage **B** solution turned reddish. Residual iron complex was removed with a 0.45 μm filter. This solution is carried forward for further characterization through ^1H NMR and FTIR spectroscopy. Fig. S6 displays a schematic respresentation of $\mathbf{2} \subset \mathbf{B}$ along with the ^1H NMR of $\mathbf{2} \subset \mathbf{B}$ (360 MHz, D_2O, 298 K): δ 9.44 (d, pyridine-Hα, cage B), 8.86 (d, pyridine-Hβ, cage B), 8.43 (d, Ha bipyridyl, cage B), 8.33 (t, Hb bipyridyl, cage B), 7.69 (d, Hd bipyridyl, cage B), 7.55 (t, Hc bipyridyl, cage B), 3.07 (s, Cp, guest 2).

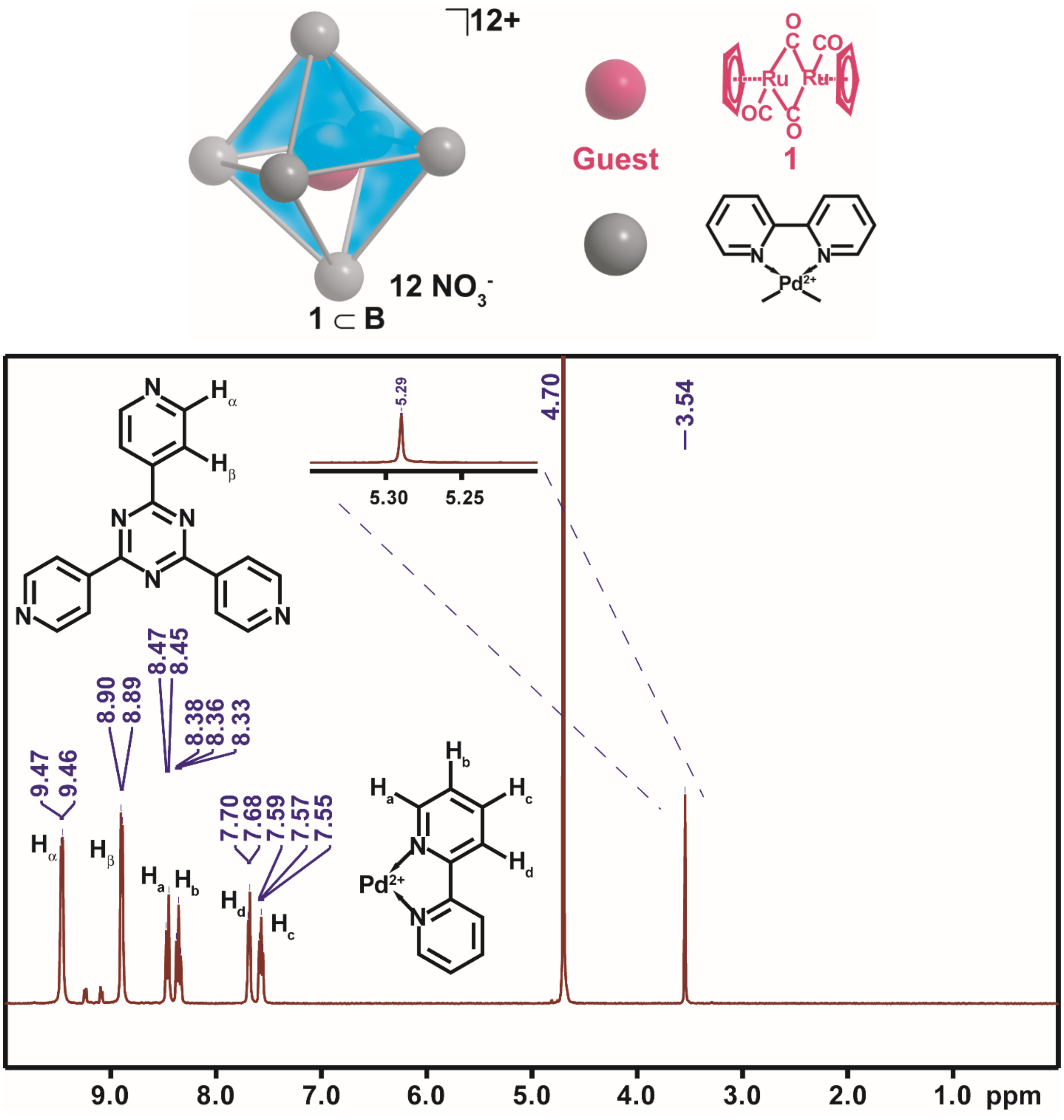

Figure S5. ^{1}H NMR spectra of **1** ⊂ **B** (360 MHz, D_2O, 298 K). Proton signals from **1** free in $CDCl_3$ (δ = 5.29 ppm, shown in inset) shift upfield, δ = 3.54 ppm (Δδ = 1.75 ppm) when **1** is encapsulated by cage **B**. The ^{1}H NMR is consistent with previously reported ^{1}H NMR spectra of a similar host-guest complex[4].

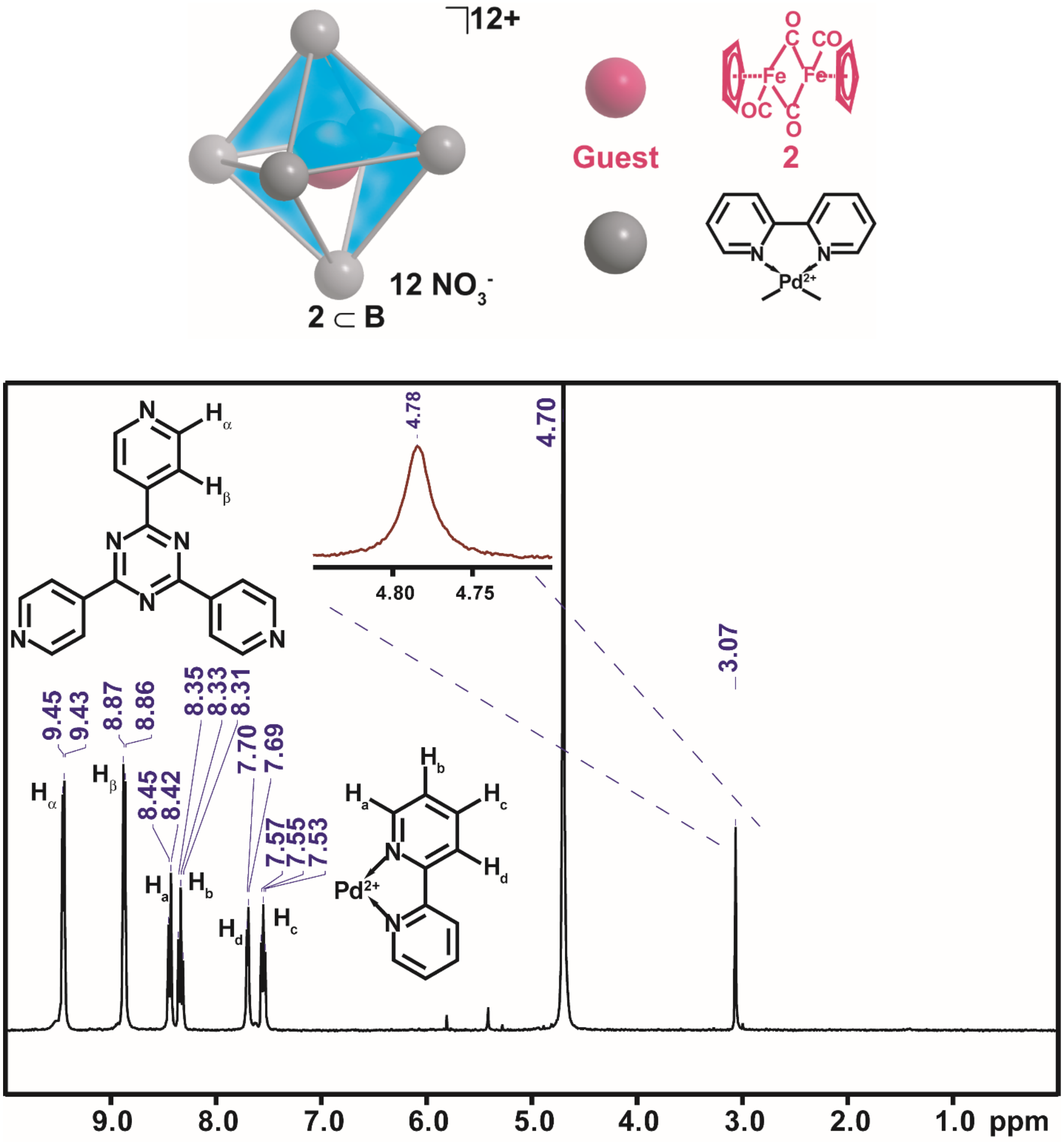

Figure S6. ^{1}H NMR spectra of **2** ⊂ **B** (360 MHz, D$_2$O, 298 K). Proton signals from **2** free in CDCl$_3$ (δ = 4.78 ppm, shown in inset) shift upfield, δ = 3.07 ppm (Δδ = 1.71 ppm) when it is encapsulated by cage **B**.

The NMR spectrum of **2⊂A** leads to the disappearance of a cyclopentadienyl proton signals associated with the guest and a broadening of the cage signals, Figure S7. We offer a few possible reasons for the disappearance of the guest signals:

1. The complex's dynamics are slowed due to incarceration.
2. The host-guests exchange dynamics have rates closer to NMR time scales.
3. Incarceration induces a change in the spin of guest **2**, from a low spin to high spin multiplicity state.

Given the fact that the size of guests **1** and **2** are very similar and the size of the hosts are also similar, in addition to the fact that the series of host-guest complexes were all prepared under identical conditions, it would be unlikely that the dynamics of only **2⊂A** would be changed. Based on this, reason **1** seems unlikely. The presence of cyclopentadienyl proton signals for **1⊂A**, **1⊂B**, and **2⊂B** along with preservation of splitting pattern for these indicates that the host-guest exchange dynamics are slower than the NMR timescales. Again, given the similarities between the systems reason 2 seems unlikely. Reason 3 suggests that the absence of the cyclopentadienyl proton signals and broadening of proton signals of cage for **2⊂A** arises from a change from a low spin to high spin state on the iron center on guest **2**. Previous work has demonstrated that changes in nearby ligands of iron based natural and biomimetic systems can result in a change in the spin state of the iron centers[5]. Based on the previous work, we attribute the absence of the cyclopentadienyl proton signal and broadening of proton signals of **2⊂A** to a change from a low spin to high spin state on the iron center on guest **2**.

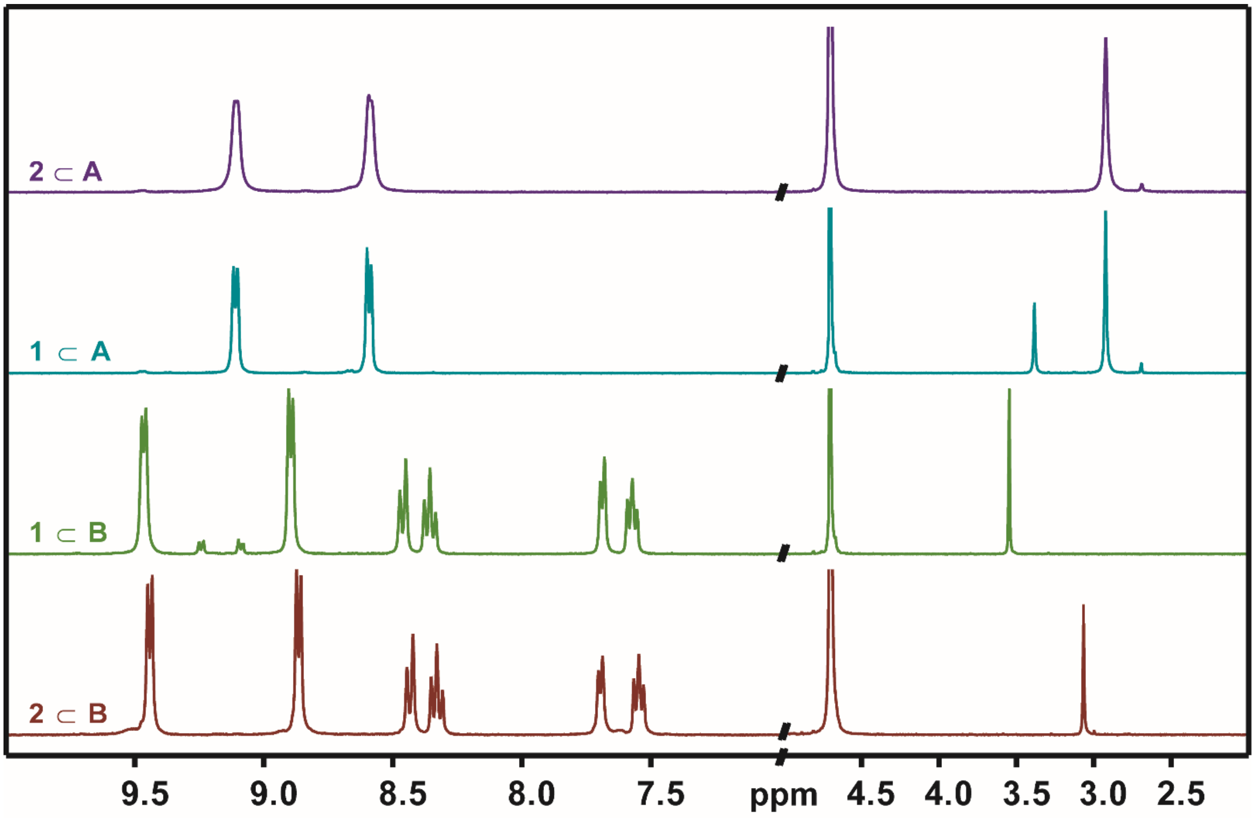

Figure S7. Comparing ^{1}H NMR spectra of **2** ⊂ **A**, **1** ⊂ **A**, **1** ⊂ **B**, **2** ⊂ **B** (360 MHz, D_2O, 298 K). Proton signals from **2** disappears when encapsulated by nanocage **A**.

4. Comparison of UV/VIS Spectra of Host, Guests, and Host-Guest Complexes

The UV/VIS absorption spectra of **1** along with cage **A**, cage **B**, **1** ⊂ **A**, and **1** ⊂ **B** are shown in Fig. S8 and of **2** along with cage **A**, cage **B**, **2** ⊂ **A**, and **2** ⊂ **B** are shown in Fig. S9. For nanocage **A** and **B**, (orange and brown lines Fig. S8-S9), the absorption is mainly in the UV region and does not extend beyond 400 nm.[3] For guests **1** and **2** the absorption features extend to the visible spectral region and are assigned to metal to ligand charge transfer states.[6-7] As can be seen in the spectra the host-guest complexes , **1** ⊂ **A**, **1** ⊂ **B**, **2** ⊂ **A**, and **2** ⊂ **B**, have contributions from the local absorption of the nanocages and the guests in addition to an emerging spectral feature. The spectra of the host-guest complexes is broader and extends beyond local absorptions of **A**, **B**, **1**, and **2**. This is attributed to the formation of a charge transfer band formed between the electron rich cyclopentadienyl groups stacked against the trispyridyl triazine walls of the cages observed in previous studies of **1** in similar Pd_6L_4 nanocages[4]. The change in the UV/VIS spectra further confirm the formation of the host-guest complexes.

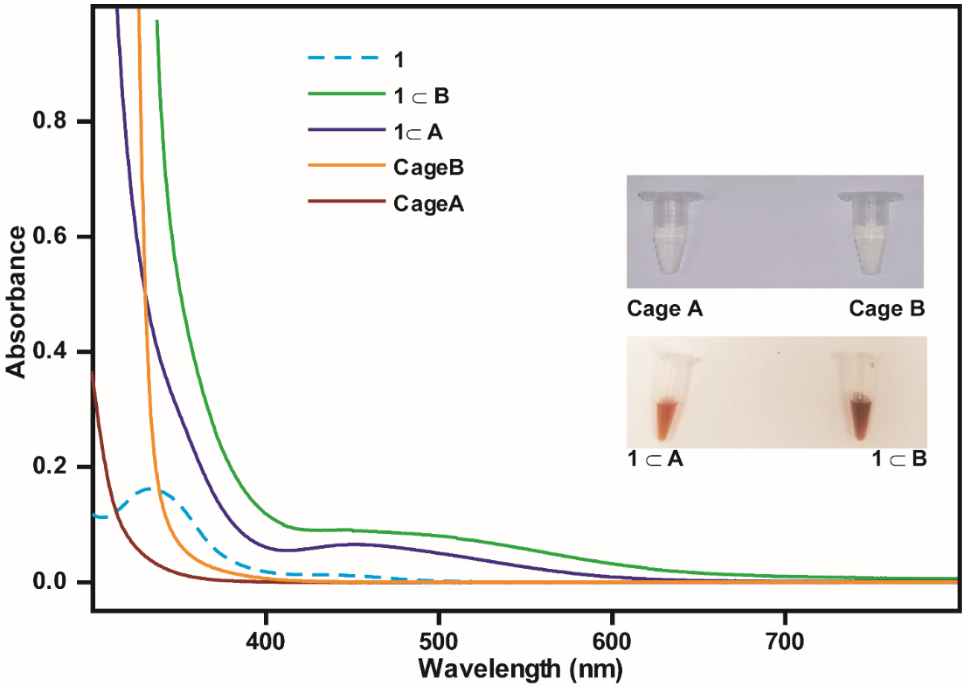

Figure S8. UV/VIS spectrum of **1** in Chloroform (dashed, cyan); **1** ⊂ **A** (solid purple); **1** ⊂ **B** (solid green); cage **A** (solid brown); cage **B** (solid orange).

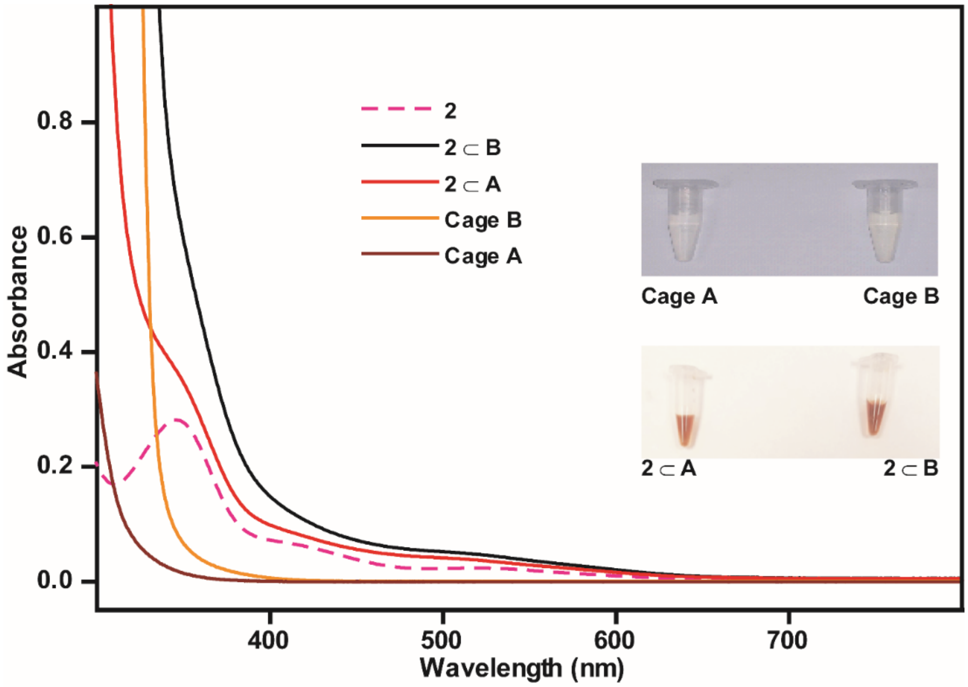

Figure S9. UV/VIS spectrum of **2** in chloroform (dashed, magenta); **2** ⊂ **A** (solid red); **2** ⊂ **B** (solid black); cage **A** (solid brown); cage **B** (solid orange).

5. Assignment of FTIR Spectra and Comparison with DFT Calculated Vibrational Modes

The FTIR spectra of **1** and **2** have been assigned previously,[8-12] and recently investigated with DFT calculations[13] (for a review article see Ref. 5 and references within) and 2DIR spectroscopy[14]. Using the optimized geometries from previous work [14], we performed frequency calculations with the Gaussian 09 software package[13] on the previously optimized DFT structures of **1** and **2** using the same functional and basis sets used previously[14]. The calculated frequencies are reported in Table S1 for **1** and **2** and are plotted as stick spectra in Fig. S10 and S11 along with the experimental FTIR spectra. For the calculated frequencies, a scaling factor of 0.962 was used for the isomers of **1** and 0.964 for the isomers of **2**.

The experimental FTIR spectrum of **1** in chloroform has four main peaks centered at 1771, 1937, 1967, and 2009 cm^{-1} arising from the contributions of four different isomers: cis-bridging, trans-bridging, trans-non-bridging and gauche-non-bridging. The different contributions to each peak are evident from comparison with the calculated stick spectra. Comparing the FTIR spectra of **1** in the cages to that of **1** in chloroform, we observe changes in the spectra with the caged system displaying two main peaks at 1745 cm^{-1} and 2001 cm^{-1}, and a smaller peak at 1958 cm^{-1}. The presence of the peak at 1745 cm^{-1} confirms that **1** exists as a bridging isomer in the encapsulated cage. In the terminal carbonyl stretching region the presence of two peaks with an intense transition at 2001 cm^{-1} and a weaker transition at 1958 cm^{-1} matches the calculated spectrum of the cis-bridging isomer. The FTIR confirm that **1** exists mainly as the cis-bridging isomer, which is consistent with previous studies of **1** in iso-structural Pd_6L_4 nanocages.[4] The FTIR spectrum of **2** in chloroform has three peaks centered at 1771, 1957, and 2002 cm^{-1} resulting from contributions of two isomers: the cis-bridging and trans-bridging forms. When encapsulated the FTIR spectra indicate that **2** remains in a bridging form. The change in the terminal carbonyl stretching region indicates that the cis-bridging isomer is stabilized upon encapsulation, with one main intense peak at 1997 cm^{-1} and a weaker peak at 1955 cm^{-1}. The trans-bridging form would only give rise to one intense transition in the terminal carbonyl region.

Table S1: DFT calculated frequencies for the different isomers of **1** and **2**. A scaling factor of 0.962 was used for **1** and a scaling factor of 0.964 was used for **2**.

Isomer	**Scaled DFT frequencies, cm^{-1} (normalized intensities)**
1	
Cis bridging	1806.1 (0.8), 1964.8 (0.2), 2001.1 (1)
Trans bridging	1806.5 (0.7), 1959.8 (1)
Gauche Non-bridging	1942.1 (0.3), 1942.5 (0.9), 1963.3 (0.6), 2008.6 (1)
Trans Non-bridging	1939.4 (1), 1962.8 (0.8)
2	
Cis bridging	1785.73 (0.8), 1968 (0.14), 2002.1 (1)
Trans Bridging	1786.3 (0.8), 1961.3 (1)

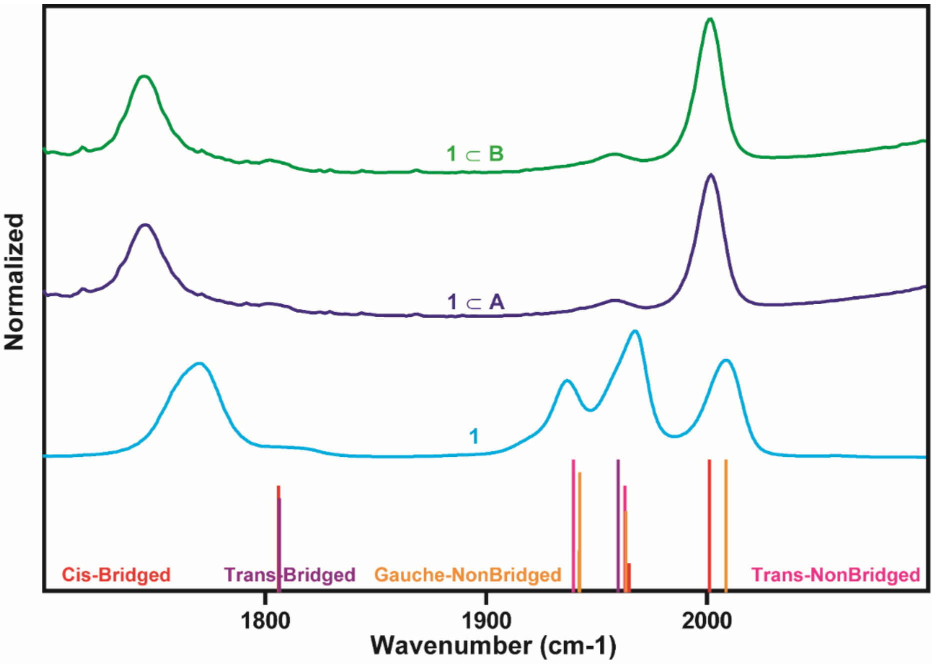

Figure S10. Experimental FTIR spectra of **1** in chloroform (cyan); **1** ⊂ **A** (violet); and **1** ⊂ **B** (green). DFT calculated stick spectra of cis-bridging isomer (red); trans-bridging isomer (purple), gauche non-bridging isomer (orange), trans non-bridging isomer (pink).

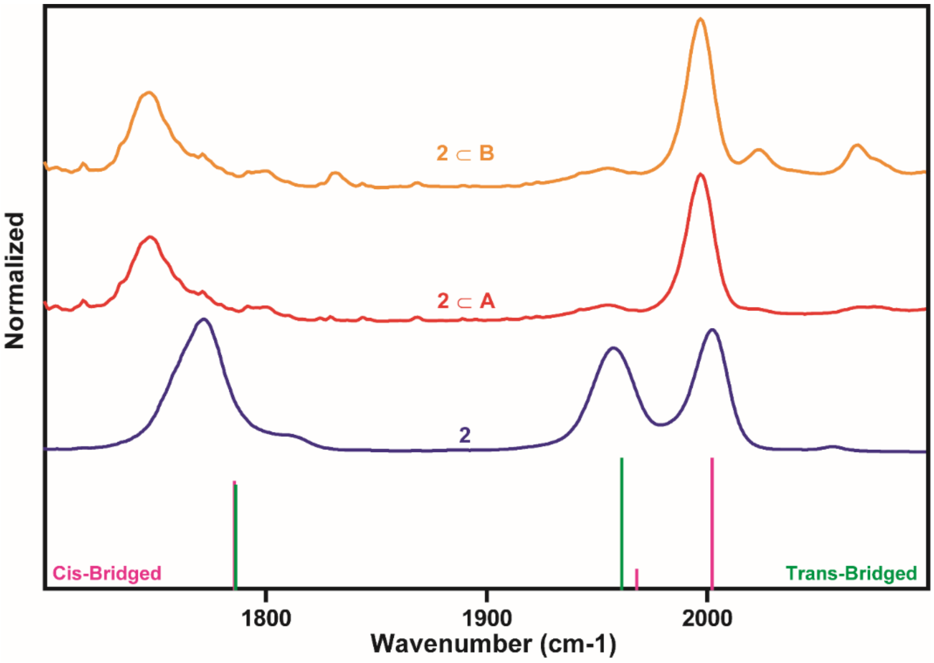

Figure S11. Experimental FTIR spectra of **2** in chloroform (purple); **2** ⊂ **A** (Red); and **2** ⊂ **B** (orange). DFT calculated stick spectra of the cis-bridging isomer (pink) and trans-bridging isomer (green).

6. Pump Probe Spectra of Guests and Host-Guest Complexes

The population dynamics and anisotropies presented in the main text were extracted from pump-probe spectra obtained under different polarization schemes. Representative pump probe spectra at varying time delays for **1** in chloroform, **1** $\subset$ **A** in D_2O, **1** $\subset$ **B** in D_2O, **2** in chloroform, **2** $\subset$ **A** in D_2O, and **2** $\subset$ **B** in D_2O are displayed in figures S12-S17.

The reported population lifetimes and anisotropy decays were obtained from polarization dependent traces of the blue-most shifted ground state bleach for each system to ensure that the traces are not contaminated by the overlap with addition ground state bleaching features and/or excited state absorptions. The time traces of the blue-edge of the highest frequency transition in the terminal carbonyl stretching region were extracted from the pump-probe spectra obtained under parallel and perpendicular polarization schemes. The traces are plotted in Fig. S18-S23.

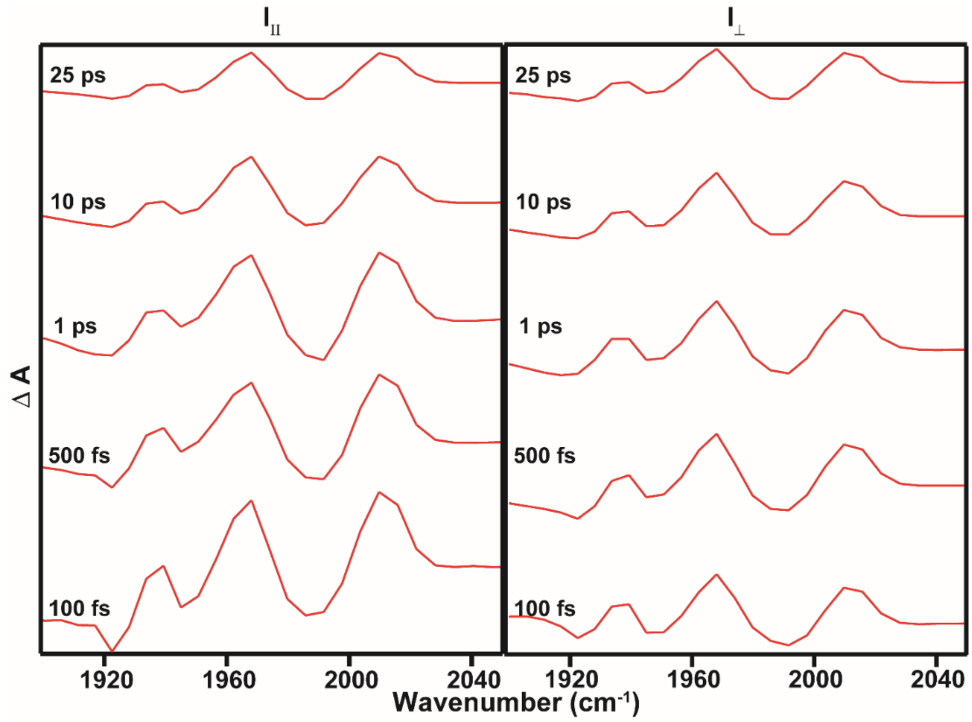

Figure S12. Mid-IR pump-probe spectra at different waiting times for **1** in chloroform performed under parallel and perpendicular polarization schemes.

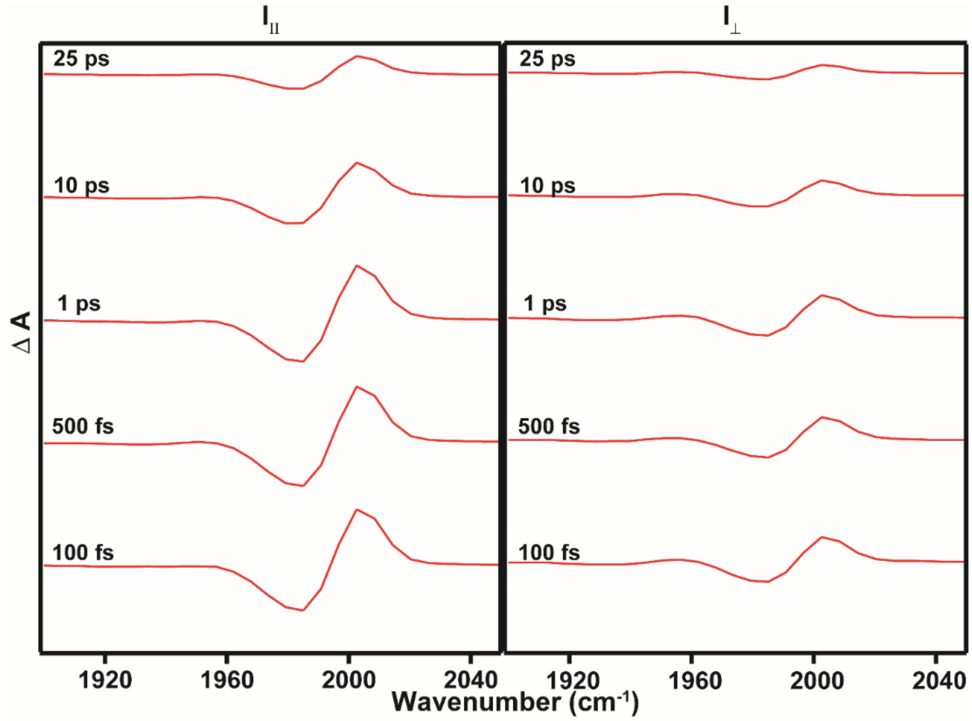

Figure S13. Mid-IR pump-probe spectra at different waiting times for **1** $\subset$ **A** in D_2O performed under parallel and perpendicular polarization schemes.

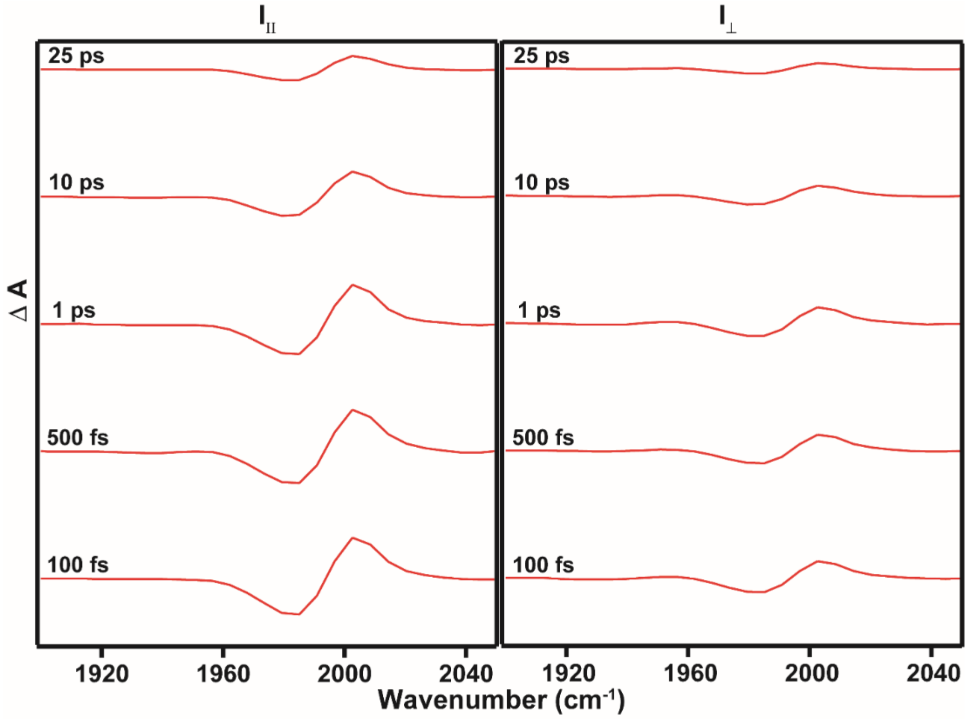

Figure S14. Mid-IR pump-probe spectra at different waiting times for **1** ⊂ **B** in D_2O performed under parallel and perpendicular polarization schemes.

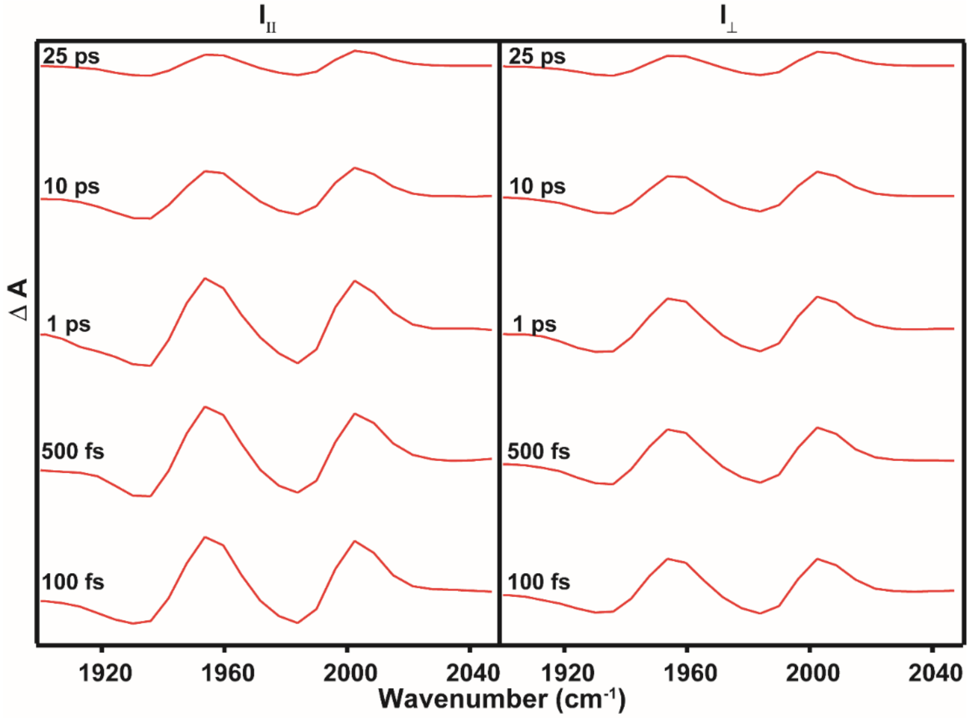

Figure S15. Mid-IR pump-probe spectra at different waiting times for **2** in chloroform performed under parallel and perpendicular polarization schemes.

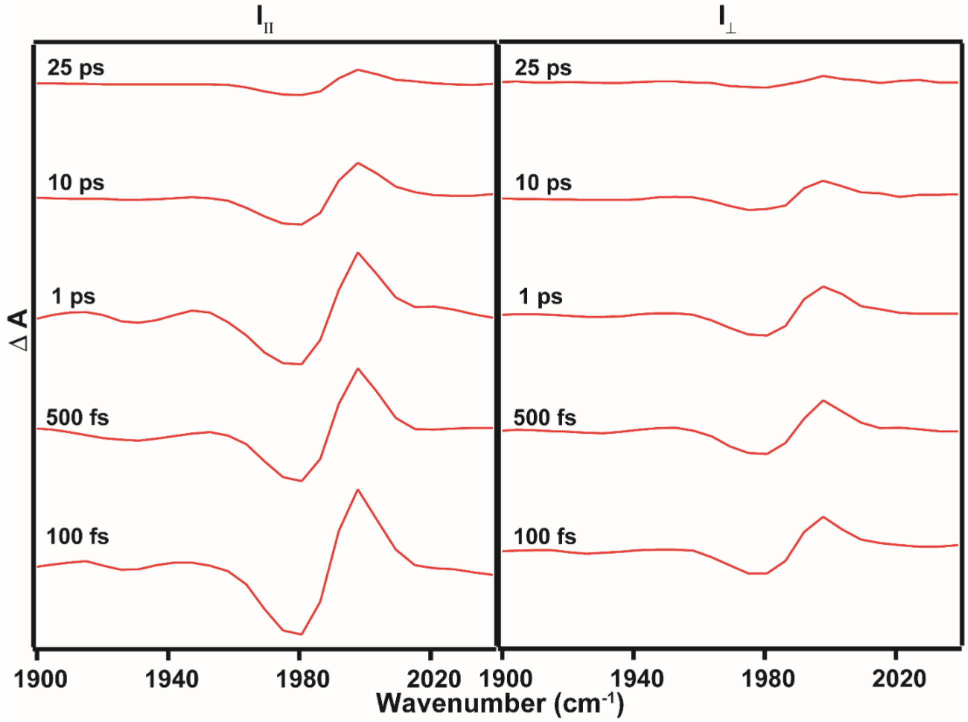

Figure S16. Mid-IR pump-probe spectra at different waiting times for **2** ⊂ **A** in D_2O performed under parallel and perpendicular polarization schemes.

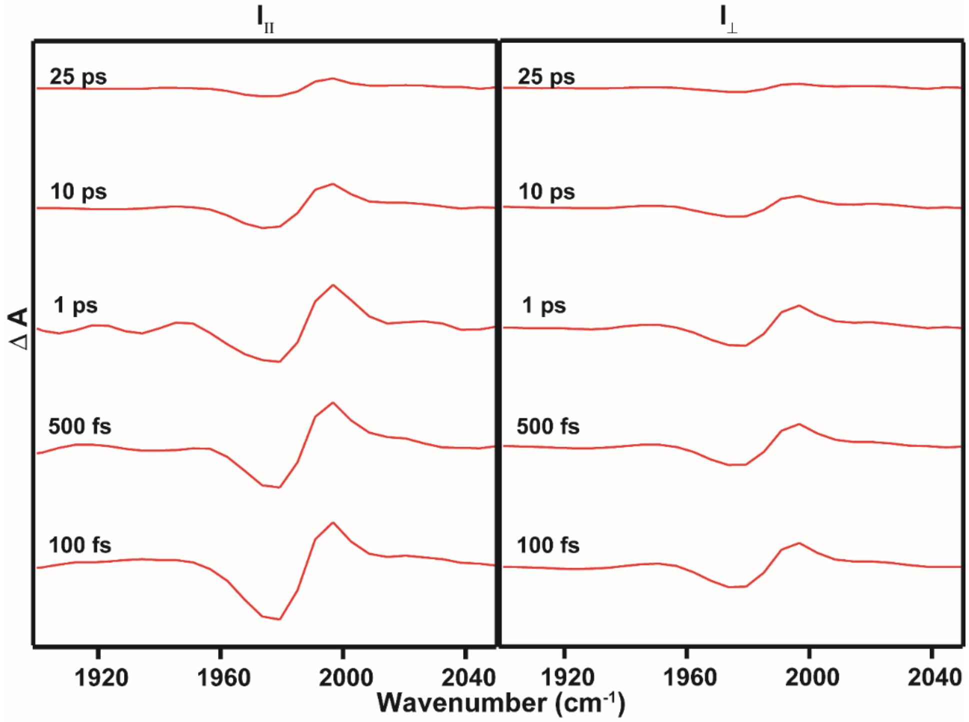

Figure S17. Mid-IR pump-probe spectra at different waiting times for **2** ⊂ **B** in D_2O performed under parallel and perpendicular polarization schemes.

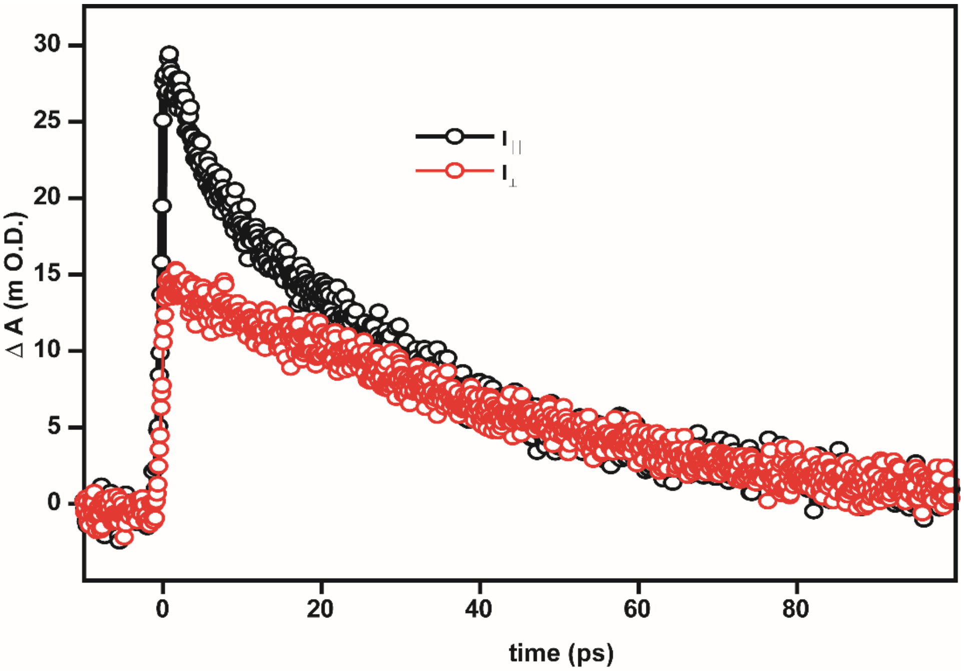

Figure S18. ΔA at 2010 cm^{-1} as a function of waiting time for the different pump polarizations $I_{||}$ (parallel) and $I_{\perp}$ (perpendicular). These traces are used to calculate the population relaxation and anisotropy decay for **1** in chloroform.

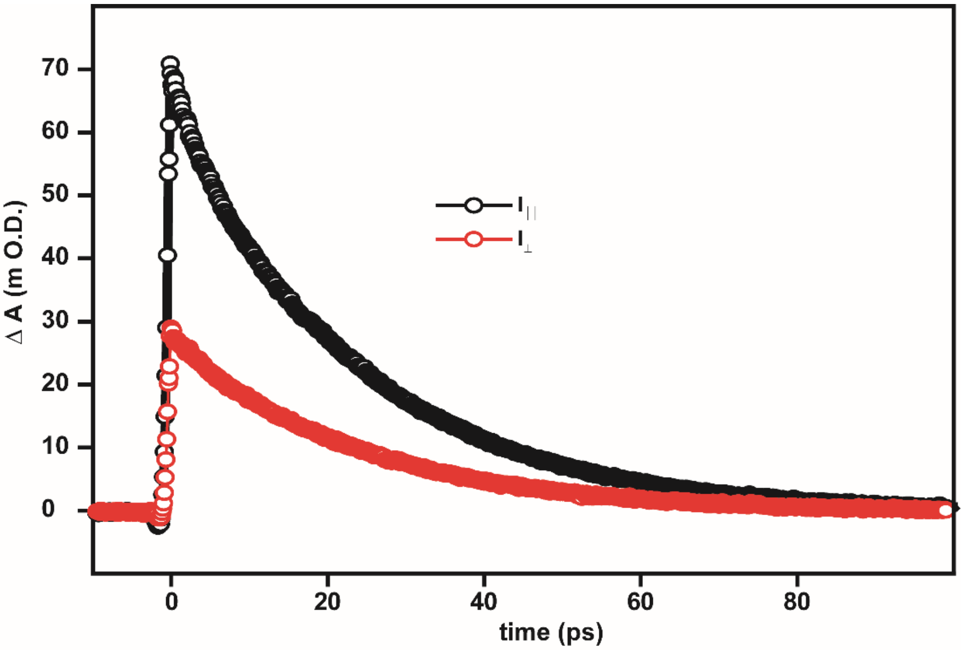

Figure S19. ΔA at 2003 cm^{-1} as a function of waiting time for the different pump polarizations $I_{||}$ (parallel) and $I_{\perp}$ (perpendicular). These traces are used to calculate the population relaxation and anisotropy decay for **1** ⊂ **A** in D_2O.

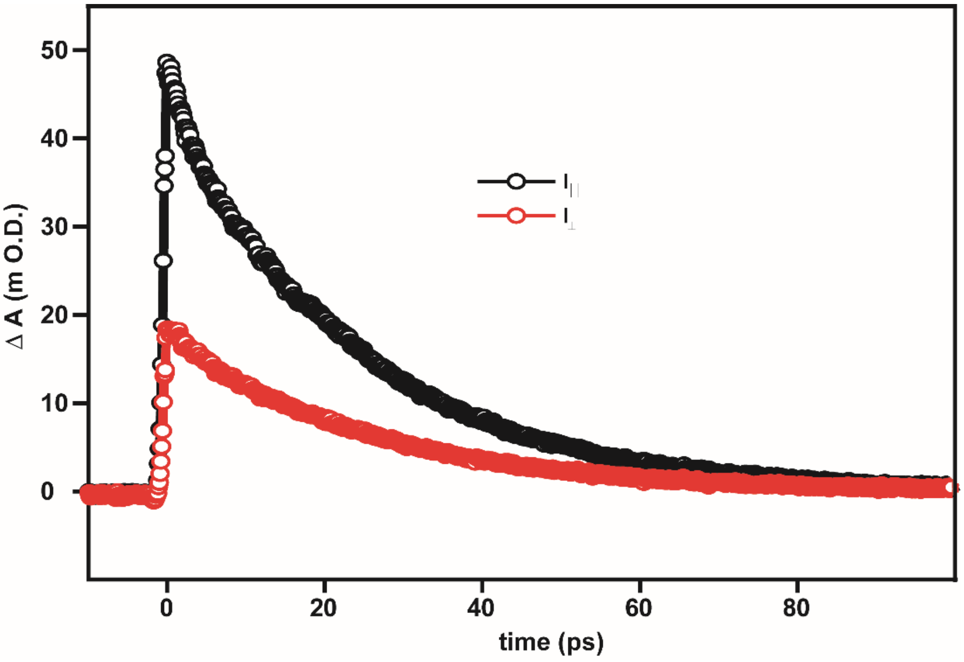

Figure S20. ΔA at 2003 cm^{-1} as a function of waiting time for the different pump polarizations I$_{||}$ (parallel) and I$_{\perp}$ (perpendicular). These traces are used to calculate the population relaxation and anisotropy decay for **1** ⊂ **B** in D$_2$O.

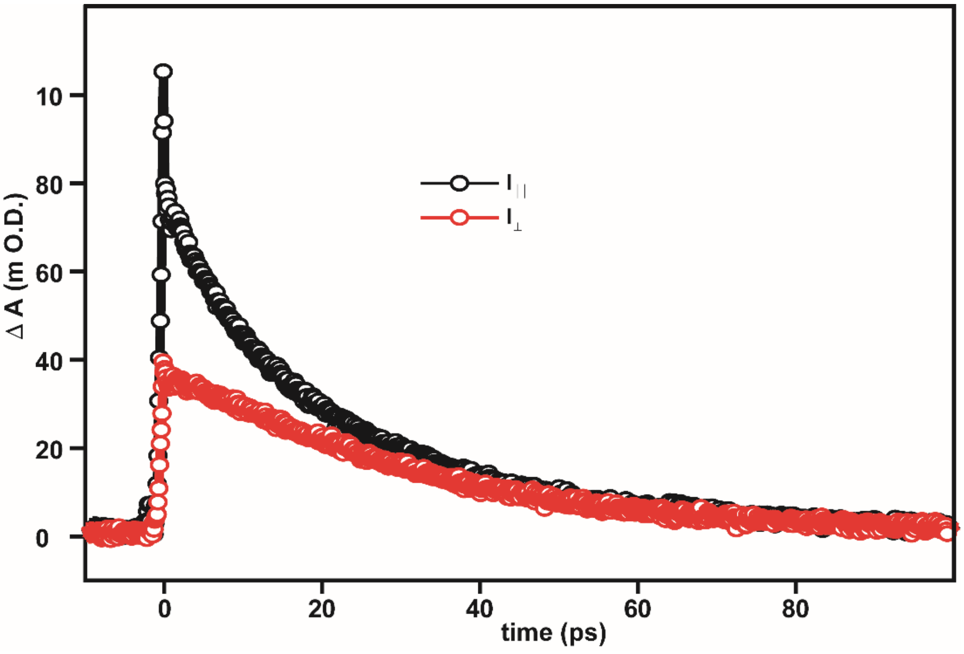

Figure S21. ΔA at 2002 cm^{-1} as a function of waiting time for the different pump polarizations I$_{||}$ (parallel) and I$_{\perp}$ (perpendicular). These traces are used to calculate the population relaxation and anisotropy decay for **2** in chloroform.

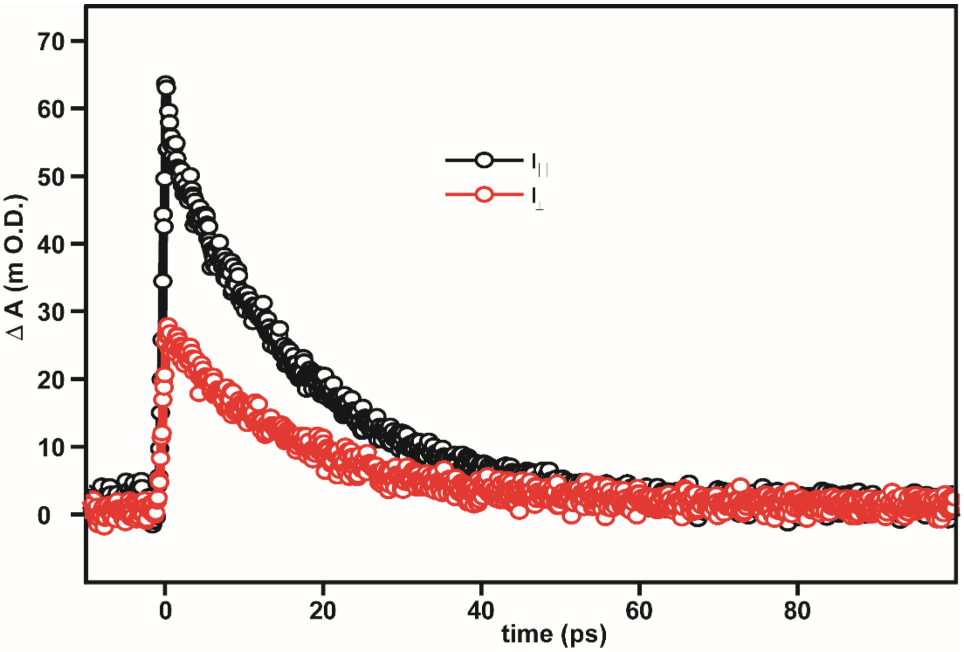

Figure S22. ΔA at 1998 cm^{-1} as a function of waiting time for the different pump polarizations $I_{\parallel}$ (parallel) and $I_{\perp}$ (perpendicular). These traces are used to calculate the population relaxation and anisotropy decay for **2** ⊂ **A** in D_2O.

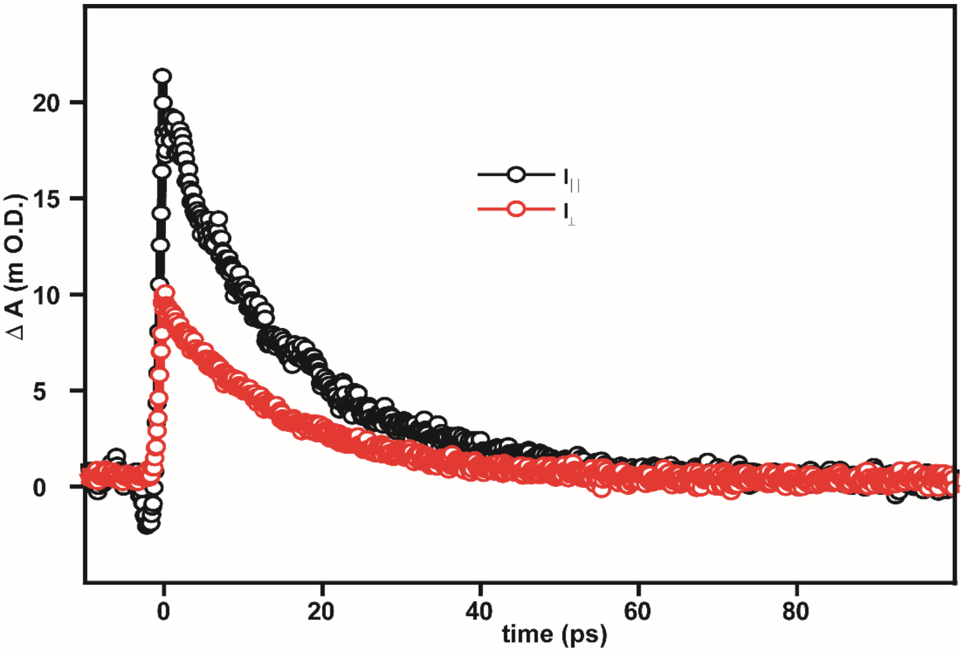

Figure S23. ΔA at 1997 cm^{-1} as a function of waiting time for the different pump polarizations $I_{\parallel}$ (parallel) and $I_{\perp}$ (perpendicular). These traces are used to calculate the population relaxation and anisotropy decay for **2** ⊂ **B** in D_2O.

7. Wobbling-In-A-Cone Model and Application to Anisotropy Data

The anisotropy, r(t), is a measure the diffusive molecular reorientation of a molecule, and is related to the dipole-dipole time correlation function according to Eq. S1 where C_2 is the dipole-dipole time correlation function (the orientational correlation function) and P_2 is the second Legendre polynomial.[15]

$$r(t) = \frac{2}{5} C_2(t) \text{ where } C_2(t) = \langle P_2[\mu(0) \cdot \mu(t)] \rangle \qquad \text{Eq. S1}$$

To experimentally obtain r(t) we performed two different measurements varying in the polarization of the pump pulse: one measurement where the pump pulse has a parallel polarization with respect to the probe pulse ($I_{\parallel}$) and the other where the pump pulse has a perpendicular polarization with respect to the probe pulse ($I_{\perp}$)). With these two measurements we obtained r(t) from Eq. S2.

$$r(t) = \frac{I_{\parallel}(\mathrm{t}) - I_{\perp}(t)}{I_{\parallel}(\mathrm{t}) + 2 * I_{\perp}(\mathrm{t})} \qquad \text{Eq. S2}$$

Plots of $I_{\parallel}$ and $I_{\perp}$ for the guests and host-guest complexes used to calculate the anisotropy are shown in Fig. S18-S23. The resulting r(t) are shown in Fig. S24 and in Fig. 4 of the main text. As the anisotropy decays the noise increases. From Fig. S18-23 the $I_{\parallel}$ and $I_{\perp}$ signal decays to zero by ~40-60 ps. For this reason, we only focus on the first 40 ps of the anisotropy data. Fig. S24 (bottom) plots the truncated anisotropy decay for **1**, **1** ⊂ **A**, **1** ⊂ **B**, **2**, **2** ⊂ **A**, **2** ⊂ **B**.

According to Eq. S1 one would expect the anisotropy of an isotropic system to be equal to 0.4 at time zero, r(0) = 0.4. We observe a deviation from this value for all the samples that we attribute to a fast relaxation process that we do not resolve due to the 120 fs temporal width of the incoming laser pulses. For a spherical isotropic system, r(t) should decay to zero with a single exponential as the molecule undergoes molecular reorientation. A single exponential fits the anisotropy decay of **1** and **2** well, giving reorientation times of 19.5 ± 7.6 ps for **1** and 11.9 ± 1.9 ps for **2**. The fits are plotted as black lines in Fig. S24, and the extracted parameters are given in Table S2.

Table S2: Parameters resulting in the best fits of the anisotropy data for **1** and **2** with a mono-exponential (A*exp(-t/τ_{or})). Error bars indicate 95% confidence intervals.

	A	τ_{or}(ps)
1	0.25 ± 0.07	19.5 ± 7.6
2	0.15 ± 0.02	11.9 ± 1.9

When metal carbonyls **1** and **2** are encapsulated in the cages the anisotropies do not decay to zero over the course of the vibrational lifetimes. Previous mid-IR pump-probe experiments performed on various probe molecules in confined environments such as membranes, polymers, and MOFs have employed a wobbling-in-cone model to interpret the anisotropy decay where angular motion of the probe molecule is restricted by the local environment.[16-20] According to the wobbling-in-a-cone model the anisotropy is given by the following expression (Eq. S3) where r_o is the anisotropy at zero time and r_∞ accounts for the non-decaying anisotropy at long times.[18-23]

$$r(t) = (r_o - r_\infty)\exp\left(-\frac{t}{\tau_\theta}\right) + r_\infty \qquad \text{Eq. S3}$$

The initial and final anisotropy values are related to the cone semi-angle (θ_c) according to the following expression, Eq. S4.[21-23]

$$\frac{r_\infty}{r_0} = [\frac{1}{2}cos\theta_c(1+\cos\theta_c)]^2 \qquad \text{Eq. S4}$$

To determine the cone semi-angles, and the extent by which the nanocages restrict the motion the metal carbonyls, we fit the anisotropy data using Eq. S3 to obtain r_∞. The fits are plotted as black lines in Fig. S24 and the optimized parameters are given in Table S3.

Table S3: Parameters resulting in the best fits of the anisotropy data for **1** ⊂ **A**, **1** ⊂ **B**, **2** ⊂ **A**, **2** ⊂ **B** with a wobbling-in-a-cone model (Eq. S3). Error bars represent 95% confidence intervals. θ_c was calculated from Eq. S4 assuming $r_0 = 0.4$ as described in the text.

	r_o	r_∞	τ_θ(ps)	θ_c
1 ⊂ A	0.327 ± 0.004	0.311 ± 0.001	3.1 ± 1.2	23.2° ± 0.1°
1 ⊂ B	0.350 ± 0.006	0.314 ± 0.002	3.3 ± 0.9	22.8° ± 0.3°
2 ⊂ A	0.318 ± 0.036	0.261 ± 0.005	0.6 ± 0.1	30.0° ± 0.7°
2 ⊂ B	0.400 ± 0.144	0.243 ± 0.004	1.70 ± 0.02	32.3° ± 0.5°

From the r_∞ values obtained from the fit, we extract an upper limit for the largest possible cone angle sampled by the metal carbonyls undergoing restricted rotational diffusion using Eq. S4. Here we assume an initial anisotropy value r_0 to be 0.4. As can be seen from the fits, we do not completely capture the ultrafast relaxation at short times for all the samples, it is for this reason that we do not use the r_0 value from the fits and focus on extracting an upper limit. Nevertheless, extracting the largest possible semi-cone angle provides insight into the restricted motion of the encapsulated metal carbonyl complexes and enables a comparison of guests **1** and **2**. The calculated semi-cone angles are also presented in Table S3 and discussed in the main text. The errors reported for the semi-cone angles were obtained by calculating the upper and lower bounds of θ_c according to the 95% confidence intervals defined by r_∞.

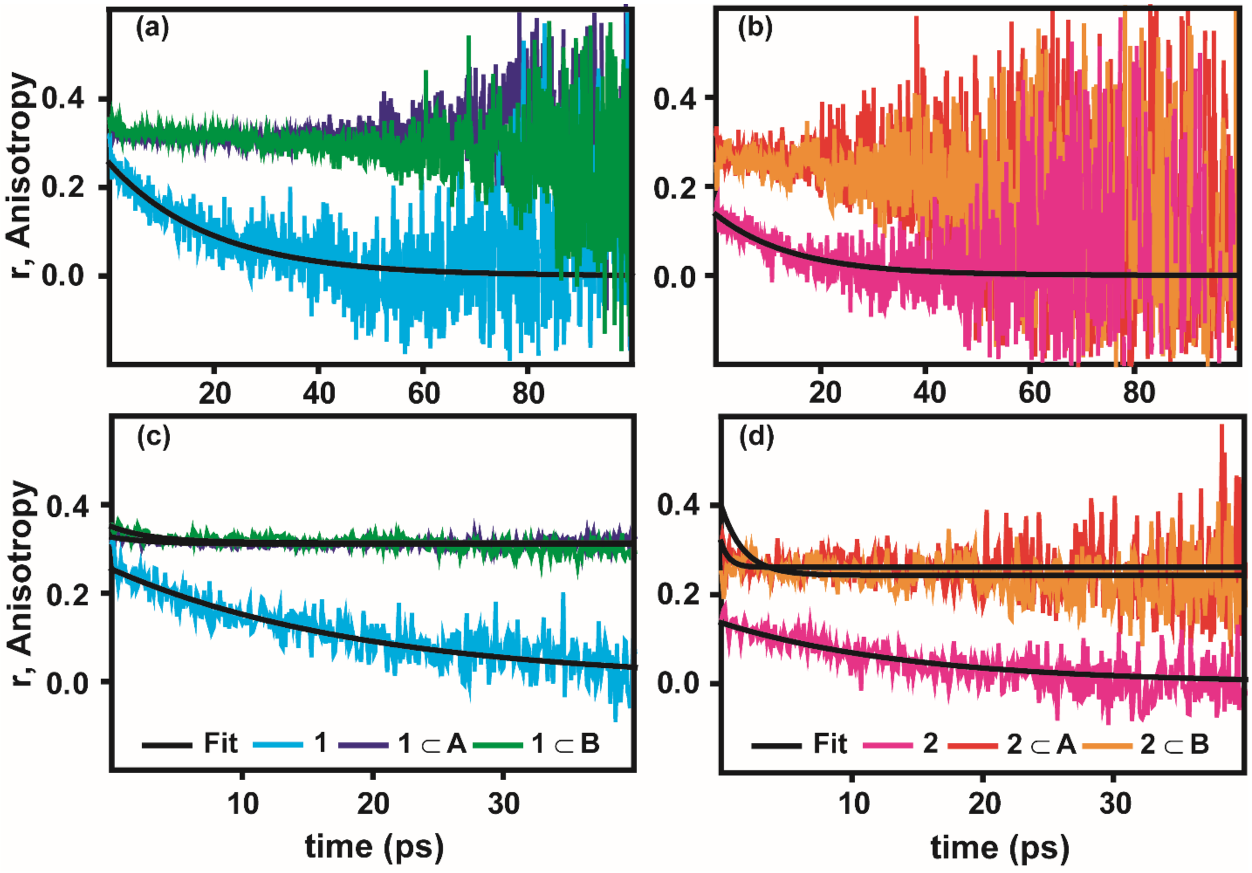

Figure S24. The anisotropy as a function of waiting time (r(t)) is plotted for **1**, **1** ⊂ **A**, and **1** ⊂ **B**, (left, a, c) and **2**, **2** ⊂ **A**, and **2** ⊂ **B**, (right, b, d). Fits are shown as solid black lines with the parameters given in Table S2 and Table S3. The truncated data is shown on the bottom.

8. References

1. Fujita, M.; Oguro, D.; Miyazawa, M.; Oka, H.; Yamaguchi, K.; Ogura, K. Self-assembly of ten molecules into nanometre-sized organic host frameworks. *Nature* **1995,** *378*, 469.
2. Kusukawa, T.; Fujita, M. Self-Assembled M6L4-Type Coordination Nanocage with 2,2'-Bipyridine Ancillary Ligands. Facile Crystallization and X-ray Analysis of Shape-Selective Enclathration of Neutral Guests in the Cage. *Journal of the American Chemical Society* **2002,** *124* (45), 13576-13582.
3. Gera, R.; Das, A.; Jha, A.; Dasgupta, J. Light-Induced Proton-Coupled Electron Transfer Inside a Nanocage. *Journal of the American Chemical Society* **2014,** *136* (45), 15909-15912.
4. Horiuchi, S.; Murase, T.; Fujita, M. Noncovalent Trapping and Stabilization of Dinuclear Ruthenium Complexes within a Coordination Cage. *Journal of the American Chemical Society* **2011,** *133* (32), 12445-12447.
5. Rebilly, J.-N.; Colasson, B.; Bistri, O.; Over, D.; Reinaud, O. Biomimetic cavity-based metal complexes. *Chemical Society Reviews* **2015,** *44* (2), 467-489.
6. Jaworska, M.; Macyk, W.; Stasicka, Z. Structure, Spectroscopy and Photochemistry of the $[M(\eta5\text{-}C_5H_5)(CO)_2]_2$ Complexes (M=Fe, Ru). In *Optical Spectra and Chemical Bonding in Inorganic Compounds: Special Volume dedicated to Professor Jørgensen I*, Mingos, D. M. P.; Schönherr, T., Eds. Springer Berlin Heidelberg: Berlin, Heidelberg, 2004; pp 153-172.
7. Abrahamson, H. B.; Palazzotto, M. C.; Reichel, C. L.; Wrighton, M. S. Photochemistry and electronic structure of bis(dicarbonyl(η5-cyclopentadienyl)ruthenium) and its iron analog. *Journal of the American Chemical Society* **1979,** *101* (15), 4123-4127.
8. Cotton, F. A.; Yagupsky, G. Tautomeric changes in metal carbonyls. I. π-Cyclopentadienyliron dicarbonyl dimer and π-cyclopentadienyl-ruthenum dicarbonyl dimer. *Inorganic Chemistry* **1967,** *6* (1), 15-20.
9. Bullitt, J. G.; Cotton, F. A.; Marks, T. J. Structural dynamic properties of pentahaptocyclopentadienylmetal dicarbonyl dimers. *Inorganic Chemistry* **1972,** *11* (4), 671-676.
10. McArdle, P.; Manning, A. R. The structures of some derivatives of dicarbonylcyclopentadienyliron dimer $[\{Fe(\pi\text{-}C_5H_5)(CO)_2\}_2]$ obtained from the reaction of pentacarbonyliron with fulvenes. *Journal of the Chemical Society A: Inorganic, Physical, Theoretical* **1970,** (0), 2119-2123.
11. McArdle, P.; Manning, A. R. The structures of dicarbonylcyclopentadienylruthenium dimer $[\{Ru(\pi\text{-}C5H5)(CO)_2\}_2]$ and some related complexes in solution. *Journal of the Chemical Society A: Inorganic, Physical, Theoretical* **1970,** (0), 2128-2132.
12. Manning, A. R. The structure of bis-π-cyclopentadienyldi-iron tetracarbonyl in solution. *Journal of the Chemical Society A: Inorganic, Physical, Theoretical* **1968,** (0), 1319-1324.
13. Frisch, M. J.; Trucks, G. W.; Schlegel, H. B.; Scuseria, G. E.; Robb, M. A.; Cheeseman, J. R.; Scalmani, G.; Barone, V.; Mennucci, B.; Petersson, G. A.; Nakatsuji, H.; Caricato, M.; Li, X.; Hratchian, H. P.; Izmaylov, A. F.; Bloino, J.; Zheng, G.; Sonnenberg, J. L.; Hada, M.; Ehara, M.; Toyota, K.; Fukuda, R.; Hasegawa, J.; Ishida, M.; Nakajima, T.; Honda, Y.; Kitao, O.; Nakai, H.; Vreven, T.; J. A. Montgomery, Jr.; Peralta, J. E.; Ogliaro, F.; Bearpark, M.; Heyd, J. J.; Brothers, E.; Kudin, K. N.; Staroverov, V. N.; Kobayashi, R.; Normand, J.; Raghavachari, K.; Rendell, A.; Burant, J. C.; Iyengar, S. S.; Tomasi, J.; Cossi, M.; Rega, N.; Millam, J. M.; Klene, M.; Knox, J. E.; Cross, J. B.; Bakken, V.; Adamo, C.; Jaramillo, J.; Gomperts, R.; Stratmann, R. E.; Yazyev, O.; Austin, A. J.; Cammi, R.; Pomelli, C.; Ochterski, J. W.; Martin, R. L.; Morokuma, K.; Zakrzewski, V. G.; Voth, G. A.; Salvador, P.; Dannenberg, J. J.; Dapprich, S.;

Daniels, A. D.; Farkas, Ö.; Foresman, J. B.; Ortiz, J. V.; Cioslowski, J.; Fox, D. J. *Gaussian 09*, Gaussian, Inc.: Wallingford CT, 2009.
14. Anna, J. M.; King, J. T.; Kubarych, K. J. Multiple Structures and Dynamics of $[CpRu(CO)_2]_2$ and $[CpFe(CO)_2]_2$ in Solution Revealed with Two-Dimensional Infrared Spectroscopy. *Inorganic Chemistry* **2011,** *50* (19), 9273-9283.
15. Gordon, R. G. Molecular Collisions and the Depolarization of Fluorescence in Gases. *The Journal of Chemical Physics* **1966,** *45* (5), 1643-1648.
16. Nishida, J.; Tamimi, A.; Fei, H.; Pullen, S.; Ott, S.; Cohen, S. M.; Fayer, M. D. Structural dynamics inside a functionalized metal–organic framework probed by ultrafast 2D IR spectroscopy. *Proceedings of the National Academy of Sciences* **2014,** *111* (52), 18442.
17. Tamimi, A.; Fayer, M. D. Ionic Liquid Dynamics Measured with 2D IR and IR Pump–Probe Experiments on a Linear Anion and the Influence of Potassium Cations. *The Journal of Physical Chemistry B* **2016,** *120* (26), 5842-5854.
18. Shin, J. Y.; Yamada, S. A.; Fayer, M. D. Dynamics of a Room Temperature Ionic Liquid in Supported Ionic Liquid Membranes vs the Bulk Liquid: 2D IR and Polarized IR Pump–Probe Experiments. *Journal of the American Chemical Society* **2017,** *139* (1), 311-323.
19. Shin, J. Y.; Yamada, S. A.; Fayer, M. D. Carbon Dioxide in a Supported Ionic Liquid Membrane: Structural and Rotational Dynamics Measured with 2D IR and Pump–Probe Experiments. *Journal of the American Chemical Society* **2017,** *139* (32), 11222-11232.
20. Yamada, S. A.; Bailey, H. E.; Tamimi, A.; Li, C.; Fayer, M. D. Dynamics in a Room-Temperature Ionic Liquid from the Cation Perspective: 2D IR Vibrational Echo Spectroscopy. *Journal of the American Chemical Society* **2017,** *139* (6), 2408-2420.
21. Kinosita, K., Jr.; Kawato, S.; Ikegami, A. A theory of fluorescence polarization decay in membranes. *Biophysical Journal* **1977,** *20* (3), 289-305.
22. Lipari, G.; Szabo, A. Effect of librational motion on fluorescence depolarization and nuclear magnetic resonance relaxation in macromolecules and membranes. *Biophysical Journal* **1980,** *30* (3), 489-506.
23. Kinosita, K., Jr.; Ikegami, A.; Kawato, S. On the wobbling-in-cone analysis of fluorescence anisotropy decay. *Biophysical Journal* **1982,** *37* (2), 461-464.